

# NUMERICAL SIMULATION OF THIN STEEL FIBER SELF-COMPACTING CONCRETE STRUCTURES

by **J. A. O. Barros, Eduardo N. B. Pereira,**  
**A. Ventura Gouveia and Álvaro F. M. Azevedo**

**Synopsis:** Steel Fiber Reinforced Self Compacting Concrete (SFRSCC) was developed and applied on the manufacture of structural façade panels composed of a grid ribbed system covered by a layer of 30 mm thickness. Panel prototypes of this structural system were tested using loading configurations that promote the flexural and the punching failure modes in order to assess the benefits of fiber reinforcement to the flexural and shear resistance of thin SFRSCC structural systems. A smeared multi-fixed crack model, implemented into a FEM-based computer program, was used to simulate the deformational behavior of the tested panel prototypes up to their failure. The fracture parameters characterizing the SFRSCC post-cracking behavior were obtained from inverse analysis, using the data derived from three point notched beam tests. The punching failure mode was well captured by adopting a softening diagram for both out-of-plane shear components.

**Keywords:** finite element method; flexural; fracture mechanics; material nonlinear analysis; punching; smeared crack model; steel fiber reinforced self-compacting concrete.

**Joaquim Barros** is Associate Professor with Aggregation and Director of the Laboratory of the Structural Group of the Department of Civil Engineering, University of Minho. He is a member of ACI Committees 440 and 544, a member of *fib* TG 9.3 and TG 8.3, and a Council member of the IIFC. His research interests include structural strengthening, composite materials, fiber reinforced concrete and finite element method.

**Eduardo Pereira** is a PhD Student in Structural Division of the Dept. of Civil Eng. of Minho University. His main interests are cement composites, from the experimental material and structural characterization to numerical modeling.

**Ventura Gouveia** is a PhD Student in Structural Division of the Dept. of Civil Eng. of Minho University. Main interests are in fiber reinforced concrete and in the development of constitutive models for the material nonlinear analysis of concrete structures.

**Álvaro Azevedo** is Assistant Professor of the Structural Division of the Faculty of Eng. of Porto University. His research interests span from finite element modeling to structural optimization.

## INTRODUCTION

Steel fiber reinforced self-compacting concrete (SFRSCC) is a relatively recent composite material which assembles the benefits of the self-compacting concrete technology (Okamura 1997) with the advantages of the fiber addition to a brittle cementitious matrix. It is a ductile material that in its fresh state flows in the interior of the formwork, filling it in a natural manner and passing through the obstacles, flowing and consolidating under the action of its own weight (Lofgren 2005, Schumacher 2006). To avoid the strong perturbation produced by steel fibers on the flowability of fresh concrete, a mix design was developed that is sensible to the fiber content, as well as to the geometrical and material properties of the fibers (Pereira 2006, Barros et al. 2007).

The developed SFRSCC was used to manufacture the lightweight panel system schematically represented in Fig 1, which can be applied in building façades. The SFRSCC mix design was optimized to assure the mechanical properties required by this structural application with a cost that is competitive when compared to the cost of glass fiber reinforced shotcrete (Barros et al. 2005). For 30 kg of fibers per concrete m<sup>3</sup>, Table 1 includes the composition that has best met self-compacting requirements (the amount of water referred does not include the aggregate's saturation water). No sign of segregation was detected, a total spread of 725 mm was measured and the mixture showed good homogeneity and cohesion, even when flowing through the small orifice of the Abrams cone (when testing, the Abrams cone was always used in the inverted position). A  $T_{50}$  of 4.6 seconds was measured (Barros et al. 2005). In the present research program RC-80/60-BN hooked ends steel fibers were used, characterized by a length ( $l_f$ ) of 60 mm, a diameter ( $d_f$ ) of 0.75 mm, an aspect ratio ( $l_f/d_f$ ) of 80 and a yield stress of 1100 MPa. Further details on this subject can be found elsewhere (Pereira 2006). At seven days the average values corresponding to the compressive strength and Young's

Modulus of the developed SFRSCC, measured in cylinders of 150 mm diameter and 300 mm height were, respectively, 52 MPa and 31 GPa.

When installed, the flexural strength of the panel is the main design concern, since the bending moments that result from wind loading cause the greatest impact for the most unfavorable load combination. To assess the panel flexural behavior, representative modules of the SFRSCC panel system were tested. Another concern of the developed panel system is its resistance to punching since, in the lightweight zones the panel is constituted by a layer that is 30 mm thick. To evaluate the punching resistance of these zones, representative modules of the panel system were submitted to a load configuration that promotes the occurrence of this type of failure mode. Two test panel prototypes were tested for each type of failure mode (Barros et al. 2005). Results of only one panel are presented for each failure mode as behavior was similar for the panels in each corresponding series. The obtained results showed that a volume percentage of 0.38 of hooked ends steel fibers provided a significant increase in terms of the maximum load and deformation capability, not only in the specimens failed in bending but also in those failed in punching (Barros et al. 2005).

Since fiber reinforcement promotes the occurrence of diffuse crack patterns, multi-fixed smeared crack models (Sena-Cruz et al. 2007) based on the nonlinear fracture mechanics (Hillerborg et al. 1976) and mesh-objectivity (Bazant and Oh. 1983) can predict with enough accuracy the behavior of this type of structures for the load configurations inducing flexural failure modes. However, simulating the behavior of laminar structures failing in punching is a much more complex task in the computational mechanics domain. 3D crack constitutive models are being proposed (Barzegar and Maddipudi 1997) but softening diagrams for modeling the II and III fracture modes (van Mier 1997) introduce numerical instabilities that, sometimes, prevent of performing the analysis of a structure up to the desired level of deformation.

In the present work, the behavior of SFRSCC plane shells failing in shear is simulated by exploring Reissner-Mindlin theory and by introducing a softening diagram for modeling both out-of-plane shear constitutive laws, immediately after crack formation. This strategy provided very accurate simulations and the computing time was much lower than the one required by full 3D crack constitutive models (implemented with solid finite elements). Another important objective of the present work is to verify the possibility of obtaining the values of the parameters that define the fracture mode I strain-softening diagram, by performing an inverse analysis with the results obtained in three point notched beam bending tests carried out according to the RILEM TC 162-TDF recommendations (RILEM 2002). From the numerical research carried out, it was verified that this strategy is valid, which has important implications on the material nonlinear analysis of FRC structures, since this indicates that the values of the fracture mode I parameters can be obtained from a test that is much more simple and faster to carry than the direct tensile test, generally recommended for assessing the fracture parameters of cement based materials.

## RESEARCH SIGNIFICANCE

The Reissner-Mindlin theory was used to simulate the behavior of thin Steel Fiber Reinforced Self Compacting Concrete panels. After crack formation, the crack constitutive laws and the out-of-plane shear stress-strain relationships were modeled by softening diagrams. Modeling the softening of both out-of-plane shear components was decisive to accurately simulate the failure mode registered in the punching tests. Another important conclusion deals with the fact that the values of the fracture mode I parameters can be obtained from inverse analysis using the force-deflection relationship obtained from three point notched beam tests carried out according to the recommendations of RILEM TC 162-TDF.

## NUMERICAL MODEL

### Formulation

To simulate the material nonlinear behavior of thin fiber reinforced concrete (FRC) structures, where out-of-plane shear deformation might be appreciable, the Reissner-Mindlin theory was selected (1945, 1951). The damage due to crack formation and propagation was simulated by discretizing the thickness of the shell in several layers. Fibers bridging micro-cracks contribute to the formation of diffuse crack patterns, since they offer resistance to the degeneration of these micro-cracks into macro-cracks. Therefore, smeared crack constitutive models are, conceptually, more appropriate than discrete crack models in the simulation of crack propagation in FRC structures, mainly in those with a great number of redundant supports (Barros and Figueiras 2001). The present paper briefly describes the multi-fixed smeared crack model that was implemented in the FEMIX 4.0 computer program, which is a software whose architecture was conceived to allow for an easy implementation of new types of finite elements and new constitutive models (Sena-Cruz *et al.* 2007). The description of the formulation will be restricted to the concrete cracked phase, for a given concrete layer, at the level of an integration point (*IP*) of a finite element, since the equations for the linear elastic phase are well known (Sena-Cruz 2004, Sena-Cruz *et al.* 2007).

For the case of cracked concrete the constitutive law is defined by the following Eq.

$$\begin{bmatrix} \Delta \underline{\sigma}_{mf} \\ \underline{\sigma}_s \end{bmatrix} = \begin{bmatrix} \underline{D}_{mf}^{crco} & \underline{0} \\ \underline{0} & \underline{D}_s^{crco} \end{bmatrix} \begin{bmatrix} \Delta \underline{\varepsilon}_{mf} \\ \underline{\varepsilon}_s \end{bmatrix} \quad (1)$$

where  $\Delta \underline{\sigma}_{mf}$  and  $\Delta \underline{\varepsilon}_{mf}$  are the vectors corresponding to the in-plane stress and strain increment components (membrane and bending):

$$\Delta \underline{\sigma}_{mf} = \{\Delta \sigma_1, \Delta \sigma_2, \Delta \tau_{12}\}^T \quad (2)$$

$$\Delta \underline{\varepsilon}_{mf} = \{\Delta \varepsilon_1, \Delta \varepsilon_2, \Delta \gamma_{12}\}^T \quad (3)$$

and  $\underline{\sigma}_s$  and  $\underline{\varepsilon}_s$  are the vectors corresponding to the out-of-plane shear stress and shear strain components, respectively:

$$\underline{\sigma}_s = \{ \tau_{23}, \tau_{31} \}^T \quad (4)$$

$$\underline{\varepsilon}_s = \{ \gamma_{23}, \gamma_{31} \}^T \quad (5)$$

In Eq. (1) the in-plane cracked concrete constitutive matrix,  $\underline{D}_{mf}^{crco}$ , is obtained by performing the following matrix operations (Sena-Cruz 2004):

$$\underline{D}_{mf}^{crco} = \underline{D}_{mf,e}^{co} - \underline{D}_{mf,e}^{co} \left[ \underline{T}^{cr} \right]^T \left( \underline{D}^{cr} + \underline{T}^{cr} \underline{D}_{mf,e}^{co} \left[ \underline{T}^{cr} \right]^T \right)^{-1} \underline{T}^{cr} \underline{D}_{mf,e}^{co} \quad (6)$$

where  $\underline{D}_{mf,e}^{co}$  is the constitutive matrix for linear-elastic concrete (Sena-Cruz 2004),  $\underline{T}^{cr}$  represents the transformation matrix from the crack local coordinate system to the element local coordinate system:

$$\underline{T}^{cr} = \begin{bmatrix} \cos^2 \theta & \sin^2 \theta & 2 \sin \theta \cos \theta \\ -\sin \theta \cos \theta & \sin \theta \cos \theta & \cos^2 \theta - \sin^2 \theta \end{bmatrix} \quad (7)$$

and  $\underline{D}^{cr}$  is the crack constitutive matrix:

$$\underline{D}^{cr} = \begin{bmatrix} D_I^{cr} & 0 \\ 0 & D_{II}^{cr} \end{bmatrix} \quad (8)$$

In Eq. (7),  $\theta$  is the angle between the crack local coordinate system and the local coordinate system of the finite element. In Eq. (8),  $D_I^{cr}$  and  $D_{II}^{cr}$  represent, respectively, the constitutive components corresponding to the crack opening mode I (normal) and crack sliding mode II (in-plane shear). The fracture mode I modulus,  $D_I^{cr}$ , is defined in Fig. 2, where  $\alpha_i$  and  $\xi_i$  are the parameters that define the shape of the crack normal stress vs. crack normal strain diagram. The ultimate crack strain ( $\varepsilon_{n,u}^{cr}$ ) is defined as a function of  $\alpha_i$  and  $\xi_i$  parameters, of fracture energy ( $G_f^I$ ), tensile strength ( $f_{ct} = \sigma_{n,I}^{cr}$ ) and crack bandwidth ( $l_b$ ), as follows (Sena-Cruz et al. 2007),

$$\varepsilon_{n,u}^{cr} = \frac{2}{\xi_1 + \alpha_1 \xi_2 - \alpha_2 \xi_1 + \alpha_2} \cdot \frac{G_f^I}{f_{ct} l_b} \quad (9)$$

where  $\alpha_1 = \sigma_{n,2}^{cr} / \sigma_{n,1}^{cr}$ ,  $\alpha_2 = \sigma_{n,3}^{cr} / \sigma_{n,1}^{cr}$ ,  $\xi_1 = \varepsilon_{n,2}^{cr} / \varepsilon_{n,u}^{cr}$  and  $\xi_2 = \varepsilon_{n,3}^{cr} / \varepsilon_{n,u}^{cr}$ .

The fracture mode II modulus,  $D_{II}^{cr}$ , is obtained from,

$$D_{II}^{cr} = \frac{\beta}{1-\beta} G_c \quad (10)$$

with

$$\beta = \left( 1 - \frac{\varepsilon_n^{cr}}{\varepsilon_{n,u}^{cr}} \right)^{p_1} \quad (11)$$

where  $\beta$  is the shear retention factor, defined as a function of the actual crack normal strain ( $\varepsilon_n^{cr}$ ) and the ultimate crack normal strain ( $\varepsilon_{n,u}^{cr}$ ), and  $G_c$  is the concrete elastic shear modulus. When a linear decrease of  $\beta$  with the increase of  $\varepsilon_n^{cr}$  is assumed, then  $p_1 = 1$ . Larger values of the exponent  $p_1$  correspond to a faster decrease of the parameter  $\beta$  (Sena-Cruz 2004). The use of a softening constitutive law to model the in-plane crack shear stress transfer can improve the accuracy of the simulation of structures failing in shear (Rots and Borst 1987). However, the simultaneous presence of softening laws to model fracture modes I and II introduces additional difficulties on assuring convergence during the loading procedure of a material nonlinear analysis.

The diagram represented in Fig. 3 was used to simulate the out-of-plane constitutive matrix,  $\underline{D}_s^{crco}$ . When the portion of concrete associated with the IP changes from uncracked to cracked state, the out-of-plane shear stresses are stored and the relation between each out-of-plane shear stress-strain ( $\tau_{23} - \gamma_{23}$  and  $\tau_{31} - \gamma_{31}$ ) follows the softening depicted in Fig. 3. Therefore, the matrix  $\underline{D}_s^{crco}$  in Eq. (1) is defined by

$$\underline{D}_s^{crco} = \begin{bmatrix} D_{III,sec}^{23} & 0 \\ 0 & D_{III,sec}^{31} \end{bmatrix} \quad (12)$$

where

$$D_{III,sec}^{23} = \frac{\tau_{23,max}}{\gamma_{23,max}} ; D_{III,sec}^{31} = \frac{\tau_{31,max}}{\gamma_{31,max}} \quad (13)$$

according to a secant approach (see Fig. 3). For each out-of-plane shear component, the peak shear strain is calculated using both the stored peak shear stress at crack initiation and  $G_c$ :

$$\gamma_{23,p} = \frac{\tau_{23,p}}{G_c} ; \gamma_{31,p} = \frac{\tau_{31,p}}{G_c} \quad (14)$$

Each out-of-plane ultimate shear strain is defined as a function of the out-of-plane peak shear strain ( $\gamma_p^{OP}$ ), the out-of-plane shear strength ( $\tau_p^{OP}$ ), the mode III (out-of-plane) fracture energy ( $G_f^{III}$ ) and the crack bandwidth ( $l_b$ ), as follows:

$$\gamma_{23,u} = \gamma_{23,P} + \frac{2G_f^{III}}{\tau_{23,p} l_b}; \quad \gamma_{31,u} = \gamma_{31,P} + \frac{2G_f^{III}}{\tau_{31,p} l_b} \quad (15)$$

In the present approach it is assumed that the crack bandwidth used for assuring mesh independence when modeling fracture mode I can also be used to define the dissipated energy in the out-of-plane fracture process.

### **Assessing the fracture mode I crack constitutive law from inverse analysis**

To obtain the values of  $\alpha_i$ ,  $\xi_i$ ,  $G_f^I$ ,  $f_{ct}$  that define the tri-linear stress-strain softening diagram (see Fig. 2), an inverse analysis was performed using the force-deflection relationships recorded in the three-point notched SFRSCC beam tests, carried out according to RILEM TC 162-TDF recommendations at the age of seven days (RILEM 2002). The inverse analysis consists on the evaluation of the values of these parameters, leading to the minimization of the ratio between the area limited by the experimental and the numerical curves (in absolute values) and the area underneath the experimental curve. The numerical curve corresponds to the results obtained by means of a FEM analysis (see Fig. 4a), where the specimen, the loading and the support conditions were simulated in agreement with the experimental flexural test setup. In this context, the specimen was discretized using a mesh of 8 noded ‘serendipity’ plane stress finite elements. The Gauss-Legendre integration scheme with 2×2 points was used in all elements, with the exception of those located at the specimen symmetry axis, where 1×2 points were used. Linear elastic material behavior was assumed in all the elements, with the exception of those located above the notch (along the specimen symmetry axis), where elastic-cracked behavior in tension was considered. The crack bandwidth,  $l_b$ , was assumed to be 5 mm, which corresponds to the width of the elements located above the notch.

In Fig. 4b the results experimentally obtained in the flexural tests are compared with those resulting from the numerical model. Although not exactly coincident, there exists a good agreement between the experimental and the numerical curves. The values assumed for the fracture parameters,  $\alpha_i$ ,  $\xi_i$ , and  $G_f^I$ , that resulted in the obtained numerical curve represented in Fig. 4b, are listed in Table 2.

## **MODEL APPRAISAL**

### **Panels failing in bending**

The flexural behavior of a lightweight SFRSCC panel was simulated with the finite element method based software above referred. The panel was discretized in a 20 by 20 mesh of 8-node layered Mindlin plane shell finite elements ( $50 \times 50 \text{ mm}^2$ ), each element

divided in 11 layers 10 mm thick (see Fig. 5b). In the panel lightweight zones, 8 of these 11 layers were assigned null rigidity to simulate the void spaces introduced by the lightweight system (polystyrene), and the other three assigned with the concrete material parameters. In rib zones, all 11 layers were assigned with concrete material parameters, being the panel total thickness 110 mm. In Fig. 5a, the lightweight elements are represented with a dark shade.

In a first examination, the simulation was executed in linear elastic regime. The structural and support scheme was defined in accordance with the representation of Fig. 5a, with the displacement orthogonal to the panel plane restrained at 8 symmetrically disposed supports. The deformational results revealed the adequacy of the model and mesh refinement defined. Assuming a linear elastic behavior for the material, a too rigid behavior was predicted by the numerical simulation. Subsequently, the simulation was executed in material nonlinear regime, assigning to concrete the constitutive properties associated with the elastic-cracked regime in tension, based on the tri-linear law parameters previously defined (see Fig. 2 and Table 2). The obtained results, when compared with the experimental ones, reveal an excessively rigid structural behavior. For the same load, the modeled behavior presents much lower deflections than those experimentally observed.

The difference between the experimental and the modeled results could be due to many distinct reasons, such as limitations of the model formulation or the inadequacy of the constitutive model. However, it appears that the difference is the result of a more relevant cause. The high structural redundancy of the panel (with 5 redundant supports) suggests that, due to imperfections in the construction of the panel (perfect flatness is hard to achieve) and the rigid character of the supports, the actual initial supports configuration is only composed by three supports needed to guarantee structural stability. The other 5 supports are, most likely, not in contact with the panel at the early stages of the test. This fact certainly reduces structural rigidity. During testing, with the load increase and the development of damaged zones, the redundant supports may gradually be activated, contacting with the panel bottom face, and the opposite may also occur, with supports losing contact with the lower panel face due to corner liftings.

To verify this eventuality, several combinations of 3 supports, among the 8 available, were considered active in distinct simulations. In one of the simulations, the configuration identified as *config. 3* (see Fig. 6) revealed a very good agreement in the initial part of the experimental behavior, indicating that this is the most probable active support configuration at the test onset. At a further stage, however, this active supports configuration starts to diverge from the experimentally observed (for an approximate load of 25 kN), revealing an excessively flexible behavior. This suggests the possibility of a new support contacting with the lower panel face, changing from idle to active state. Once again, some simulations were performed to confirm this hypothesis, turning into active each of the 5 idle supports. As shown in Fig. 7, *config. 4* exhibited a good agreement with the experimental observation up to a load of approximately 35 kN, becoming also too flexible for a higher load. Again, this situation suggested the activation of another support, and *config. 5* was the new supports configuration that best adjusted to

the experimentally observed behavior. This configuration revealed a good agreement up to a load of approximately 50 kN, and started to diverge not by excessive flexibility, as before, but by excessive rigidity, suggesting that, instead of having a new support changing from idle to active, a change from active to idle would be probable. In fact, the simulation results revealed one of the supports changing its reaction sign from positive to negative. The alteration of its status from active to idle resulted in *config. 6*, and this last configuration revealed good correlation with experimental results at the plateau-softening stage of the panel behavior.

The final crack pattern estimated by the numerical model at the bottom panel face is represented in Fig. 8a. Comparing this pattern with the one revealed by the photo taken of the bottom face at the end of the panel test (see Fig. 8b), an overall good agreement between the modeled behavior and the experimental results can be observed. The major flexure cracks are predicted by the model, and the accuracy reached by the model is perfectly acceptable if one considers the random effect of a not perfectly homogeneous distribution of steel fibers in a bisymmetric structure. Eventually, the sequence of active supports configuration estimated by the model is coincident with the experimentally obtained, being this statement supported not only by Fig. 8a and 8b, but also by the agreement reached between the experimental and numerical curves represented in Fig. 7. The panel structural behavior showed an improved ability to redistribute stresses and to retain high bearing ability even for high damage levels. Though in a small amount ( $30 \text{ kg/m}^3$ ), steel fibers conferred to the panel an improved toughness, thus exhibiting a great deformation ability without loss of structural integrity and a ductile structural behavior.

#### **Panels failing in punching**

The performance of the proposed constitutive model is also assessed by simulating a punching test with a panel prototype that is representative of the developed lightweight panel system (Barros et al. 2004, Barros et al. 2005). The test layout and the test setup are represented in Fig. 9. The finite element idealization, load and support conditions used in the numerical simulation of the punching test are shown in Fig. 10. Only one quarter of the panel was used in the simulation due to double symmetry. Serendipity 8 noded Mindlin shell layered elements with  $2 \times 2$  Gauss-Legendre integration scheme were used. The panel thickness of 110 mm was decomposed in 11 layers of equal thickness. In the lightweight zone (shaded elements in Fig. 10) the first 9 layers correspond to the polystyrene material (null strength and null stiffness) and only the last 3 layers correspond to SFRSCC. The dashed line represents the support of the panel, which was simulated with line springs with “infinite” stiffness in compression and null strength in tension, in order to simulate the loss of contact between the panel and the support during the loading process.

The concrete properties used in the simulation of the punching test are listed in Table 2. To evaluate the performance of the proposed model two numerical simulations were carried out. The first simulation considers a linear behavior for both out-of-plane shear components. The second simulation considers a softening behavior in both out-of-plane shear components when the SFRSCC cracks. In Fig. 11 the numerically obtained

relations between the force and the deflection in the center of the tested panel are compared with the one recorded in the experimental test. In this figure it can be observed that both numerical simulations have practically the same pre-peak response. However, the post-peak response differs significantly. If a linear behavior is assumed for both out-of-plane shear components the force increases up to 60 kN. Moreover, a structural softening only occurs for a deflection of 9.6 mm, with a very smooth load decay. The behavior predicted by this numerical simulation after a deflection of about 3 mm differs significantly from the experimental response. When a softening behavior in both out-of-plane shear components is adopted, the numerical model predicts with high accuracy the behavior that was experimentally observed. The value of the mode III fracture energy used to define the out-of-plane shear stress-strain softening diagram has no experimental support. This value was estimated in order to assure the abrupt load decay observed experimentally at a deflection of about 3 mm, resulting a value of  $G_f^{III} = 3.0 \text{ N/mm}$ . Increasing  $G_f^{III}$  leads to the occurrence of the abrupt load decay at a larger deflection.

To estimate the contribution of fiber reinforcement to the punching resistance, a numerical simulation was performed adopting for the fracture mode I the parameters indicated in Table 2, which correspond to plain concrete of compressive strength matching the developed SFRSCC. Comparing the curves in Fig. 11 it can be concluded that fibers not only increased significantly the punching resistance, but also, and especially, improved the ductility.

Fig. 12 represents the vertical displacement field for a deflection of 10 mm in the center of the panel for the case of the numerical simulation considering out-of-plane shear softening. The accentuated gradient of vertical displacements matches with high precision the experimentally observed location of the interception of the punching failure surface with the top panel face (see Fig. 13). This evidences the capability of the developed approach in simulating this complex failure mode.

## CONCLUSIONS

A high performance and cost competitive steel fiber reinforced self-compacting concrete (SFRSCC) was developed and applied in the construction of lightweight panels that can be used in building façades. To assess the contribution of fiber reinforcement to the flexural and punching resistance of this structural system, series of experimental tests with representative modules were carried out using test setups that promote flexural and punching failure modes. In this phase of the project, 30 kg of hooked end steel fibers per concrete cubic meter were used. It could be verified that this content of fibers increased significantly the flexural and the punching resistance of the structural system.

To simulate the behavior of the tested panels, a smeared crack constitutive model was implemented in the FEMIX 4.0 computer code, using the Reissner-Mindling theory and the layer concept for the material nonlinear analysis of plane shell structures. Performing an inverse analysis with the force-deflection curves obtained in three-point notched beam

tests carried out according to RILEM TC 162-TDF recommendations, it was verified that this is a valid strategy to obtain the values of the fracture parameters that define the normal stress-strain crack constitutive relationship. This is a relevant point since this type of test is much more simple and faster to execute than the direct tensile test that is recommended to determine the values of the fracture mode I parameters of cement based materials.

To simulate the out-of-plane strain gradient that occurs in punching tests, a softening diagram was proposed to model, after crack initiation, both out-of-plane shear stress-strain constitutive laws.

The model performance was appraised by using the results obtained in the flexural and punching tests with lightweight panel prototypes of SFRSCC. A very good agreement between the experimental results and the proposed model was observed.

### ACKNOWLEDGEMENTS

The authors wish to acknowledge the support provided by the Portuguese Science and Technology Foundation (FCT) by means of the project POCTI/ECM/57518/2004 “FICOFIRE - High performance fiber reinforced concrete of enhanced fire resistance”. The third author acknowledges the financial support of FCT, PhD Grant number SFRH/BD/23326/2005.

### NOTATION

$\underline{D}$	=	constitutive matrix
$\underline{D}^{cr}$	=	crack constitutive matrix
$D_I^{cr}$	=	crack constitutive matrix component relative to the crack normal opening mode (mode I)
$D_{II}^{cr}$	=	crack constitutive matrix component relative to the crack in-plane sliding mode (mode II)
$\underline{D}_{mf,e}^{co}$	=	constitutive matrix of in-plane membrane and bending components for concrete in elastic regime
$\underline{D}_{mf}^{crco}$	=	constitutive matrix of in-plane membrane and bending components for cracked concrete
$\underline{D}_s^{crco}$	=	constitutive matrix of out-of-plane shear components for cracked concrete
FRC	=	fiber reinforced concrete
$G_c$	=	concrete transverse elasticity modulus
$G_f^I$	=	mode I (in-plane) fracture energy
$G_f^{III}$	=	mode III (out-of-plane) fracture energy
SFRSCC	=	steel fiber reinforced self compacting concrete

$T_{50}$	=	time to reach a spread diameter of 500 mm on the spread flow test
$T^{cr}$	=	transformation matrix from crack local coordinate system to element local coordinate system
$d_f$	=	steel fiber diameter
$f_{ct}$	=	tensile strength
$l_b$	=	crack band width
$l_f$	=	steel fiber length
$p_l$	=	shear degradation factor
$\alpha_i$	=	fracture parameters used to define the tri-linear stress-strain softening diagram
$\beta$	=	shear retention factor
$\Delta \underline{\varepsilon}_{mf}$	=	vector containing the in-plane membrane and bending strain increment components
$\varepsilon_n^{cr}$	=	crack normal strain
$\varepsilon_{n,u}^{cr}$	=	ultimate crack normal strain
$\underline{\varepsilon}_s$	=	vector containing the out-of-plane shear strain components
$\gamma_p^{OP}$	=	out-of-plane peak shear strain
$\gamma_u^{OP}$	=	out-of-plane ultimate shear strain
$\gamma_{max}^{OP}$	=	maximum out-of-plane shear strain in softening branch
$\theta$	=	angle between the crack local coordinate system and the element local coordinate system
$\xi_i$	=	fracture parameters used to define the tri-linear stress-strain softening diagram
$\Delta \underline{\sigma}_{mf}$	=	vector containing the in-plane membrane and bending stress increment components
$\sigma_n^{cr}$	=	crack normal stress
$\underline{\sigma}_s$	=	vector containing the out-of-plane shear stress components
$\tau_p^{OP}$	=	out-of-plane shear strength
$\tau_{max}^{OP}$	=	maximum out-of-plane shear stress in softening branch
$\nu$	=	poisson coefficient

## REFERENCES

- Barros, J.A.O.; Pereira, E.B.; Santos, S.P.F., "Lightweight panels of steel fiber reinforced self-compacting concrete", *Journal of Materials in Civil Engineering*, 19(4), 295-304, 2007.
- Barros, J.A.O. et al., "PABERFIA- Lightweight sandwich panels in steel fiber reinforced self compacting concrete", Technical report 05-DEC/E-29, Dep. Civil Eng., School Eng. University of Minho, 63 p., November 2005.

Barros, J.A.O.; Pereira, E.B.; Ribeiro, A.F.; Antunes J.A.B., "Self-compacting steel fibre reinforced concrete for precasted sandwich panels – experimental and numerical research", Workshop of 6th International RILEM Symposium on fibre reinforced concrete - BEFIB 2004, 24-25 September 2004.

Barros, J.A.O.; Figueiras, J.A. "Nonlinear analysis of steel fibre reinforced concrete slabs on grade", *Computers & Structures Journal*, 79(1), 97-106, January 2001.

Barzegar, F.; Maddipudi, S., "Three-dimensional modeling of concrete structures. I: plain concrete", *Journal of structural engineering*, 123(10), 1339-1347, 1997.

Bazant, Z.P.; Oh, B.H., "Crack band theory for fracture of concrete", *Materials and Structures, RILEM*, 16(93), 155-177, 1983.

Hillerborg, A.; Modéer, M.; Petersson, P.E., "Analysis of crack formation and crack growth in concrete by means of fracture mechanics and finite elements", *Cement and Concrete Research*, Vol. 6, 773-782, 1976.

Lofgren, I., "Fibre-reinforced Concrete for Industrial Construction", PhD Thesis, Department of Civil and Environmental Engineering, Chalmers University of Technology, Sweden, 2005.

Mindlin, R.D., "Influence of rotary inertia and shear on flexural motions of isotropic, elastic plates", *Jour. of Appl. Mech.*, 18(1), *Trans. ASME*, Vol. 73, 31-38, 1951.

Okamura, H., "Ferguson Lecture for 1996: Self-compacting high-performance concrete", *Concrete International, ACI* 19(7), 50-54, 1997.

Pereira, E.N.B., "Steel Fibre Reinforced Self-compacting Concrete: from material to mechanical behaviour", dissertation for Pedagogical and Scientific Aptitude Proofs, Department Civil Engineering, University of Minho, 188 pp, 2006.  
<<http://www.civil.uminho.pt/composites>>

Reissner, E., "The effect of transverse shear deformation on the bending elastic plates", *Jour. Appl. Mech.*, 12, 69-76, 1945.

RILEM TC 162-TDF, "Test and design methods for steel fibre reinforced concrete - Final Recommendation", *Materials and Structures* 35(253), 579-582, 2002.

Rots, J.G. and de Borst, R., "Analysis of mixed-mode fracture in concrete", *Journal of Engineering Mechanics, ASCE*, 113(11), 1739-1758, 1987.

Schumacher, P., "Rotation capacity of self-compacting steel fiber reinforced concrete", PhD Thesis, Delft University of Technology, 2006.

Sena-Cruz, J.M., “Strengthening of concrete structures with near-surface mounted CFRP laminate strips”, PhD Thesis, Department of Civil Engineering, University of Minho, 2004. <<http://www.civil.uminho.pt/composites>>

Sena-Cruz, J.M.; Barros, J.A.O.; Azevedo, A.F.M.; Ventura-Gouveia, A., “Numerical simulation of the nonlinear behavior of RC beams strengthened with NSM CFRP strips“, CMNE/CILAMCE, FEUP, Porto, 13, 13-15 June, 2007.

van Mier, J.G.M., “Fracture Processes of Concrete”, CRC Press, 1997.

Table 1 -- Final composition for 1 m<sup>3</sup> of SFRSCC including 30 kg/m<sup>3</sup> of fibers.

Paste Total volume (%)	Cement CEM I 42.5R (kg)	Limestone filler (kg)	Water (dm <sup>3</sup> )	Super-plasticizer* (dm <sup>3</sup> )	Fine sand (kg)	Coarse sand (kg)	Crushed aggregates (kg)
0.34	364.28	312.24	93.67	6.94	108.59	723.96	669.28

\* Third generation based on polycarboxilates (Glenium® 77SCC)

Table 2 -- Concrete properties used in the numerical simulations of the panel prototypes.

Poisson's ratio	$\nu = 0.15$
Initial Young's modulus	$E_c = 31000.0 \text{ N/mm}^2$
Compressive strength	$f_c = 52.0 \text{ N/mm}^2$
Tri-linear tension softening diagram of plain concrete	$f_{ct} = 3.5 \text{ N/mm}^2$ ; $G_f^I = 0.08732 \text{ N/mm}$ ; $\xi_1 = 0.072$ ; $\alpha_1 = 0.15$ ; $\xi_2 = 0.4432$ ; $\alpha_2 = 0.09$
Tri-linear tension softening diagram of SFRSCC	$f_{ct} = 3.5 \text{ N/mm}^2$ ; $G_f^I = 4.3 \text{ N/mm}$ ; $\xi_1 = 0.009$ ; $\alpha_1 = 0.5$ ; $\xi_2 = 0.15$ ; $\alpha_2 = 0.59$
Fracture energy (Mode III) used in the out-of-plane stress-shear diagram	$G_f^{III} = 3.0 \text{ N/mm}$
Parameter defining the mode I fracture energy available to the new crack	$p_2 = 2$
Shear retention factor	<i>Exponential</i> ( $p_1 = 2$ )
Crack bandwidth	<i>Square root of the area of the integration point</i>
Threshold angle	$\alpha_{th} = 30^\circ$

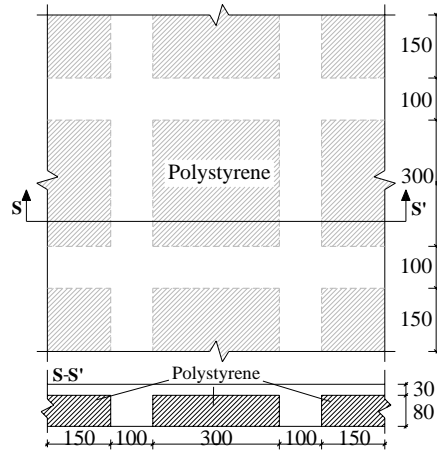


Fig. 1 -- Concept of a lightweight steel fiber reinforced self-compacting concrete panel (dimensions in mm).

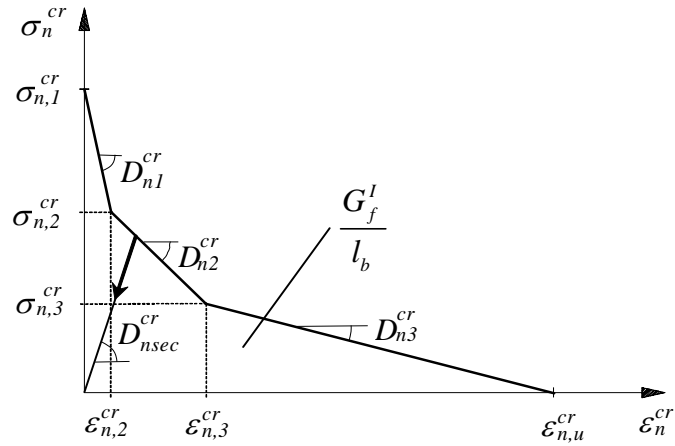


Fig. 2 -- Tri-linear stress-strain diagram for modeling the fracture mode I.

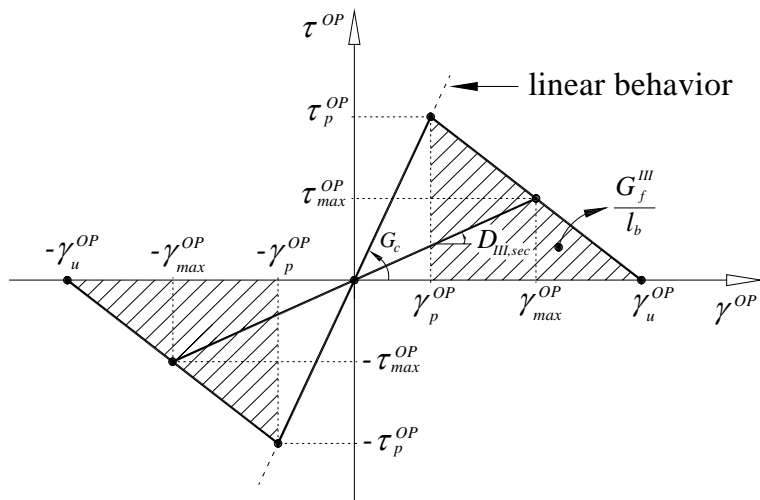


Fig. 3 -- Generic out-of-plane (OP) shear stress-strain diagram.

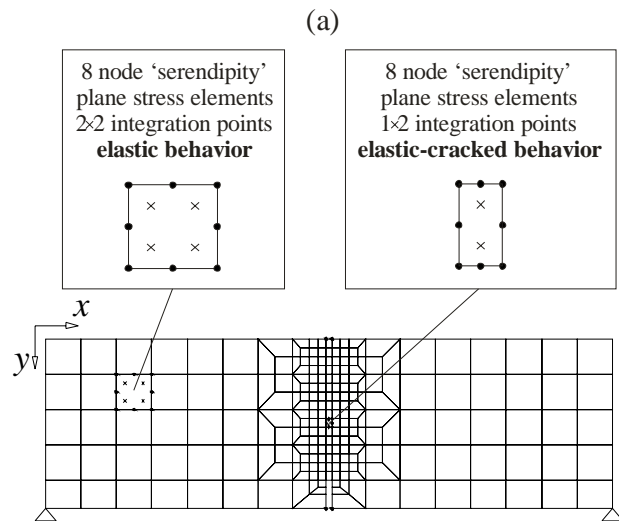


Fig. 4 -- Three-point notched beam flexural test at 7 days: (a) FEM mesh used in the numerical simulation (cont.).

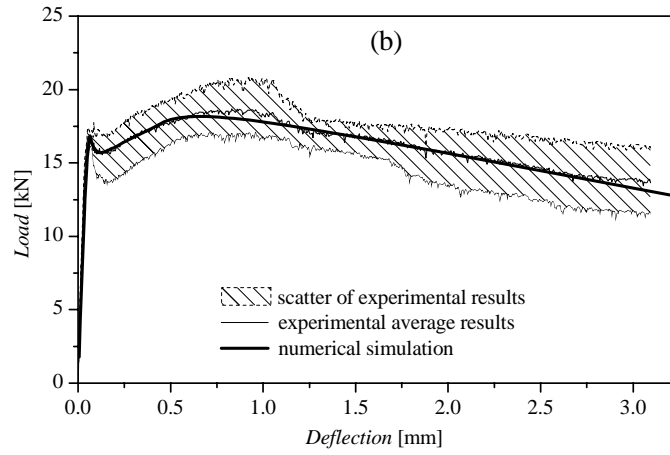


Fig. 4 (cont.) -- Three-point notched beam flexural test at 7 days: (b) obtained results.

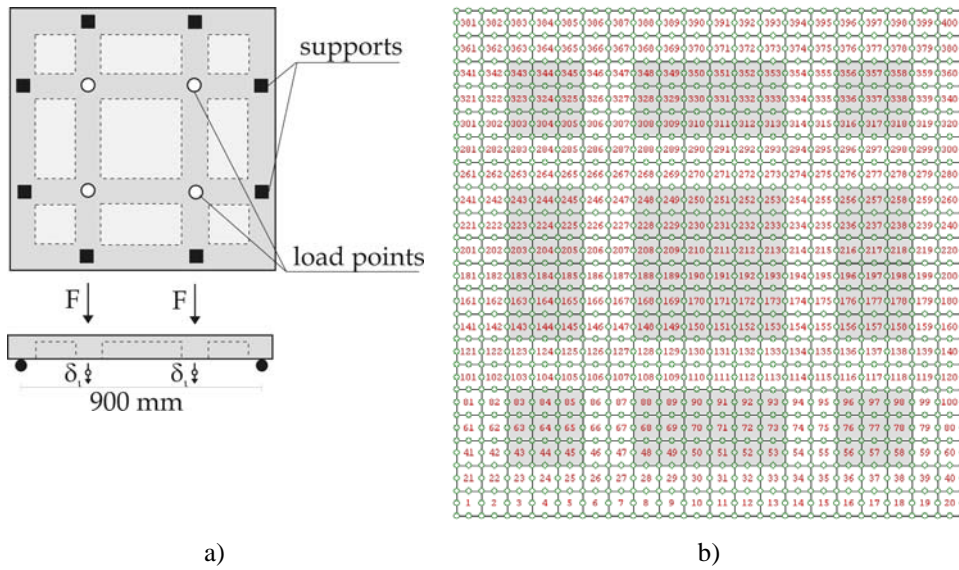


Fig. 5 -- a) Setup of the flexural panel test and b) finite element mesh.

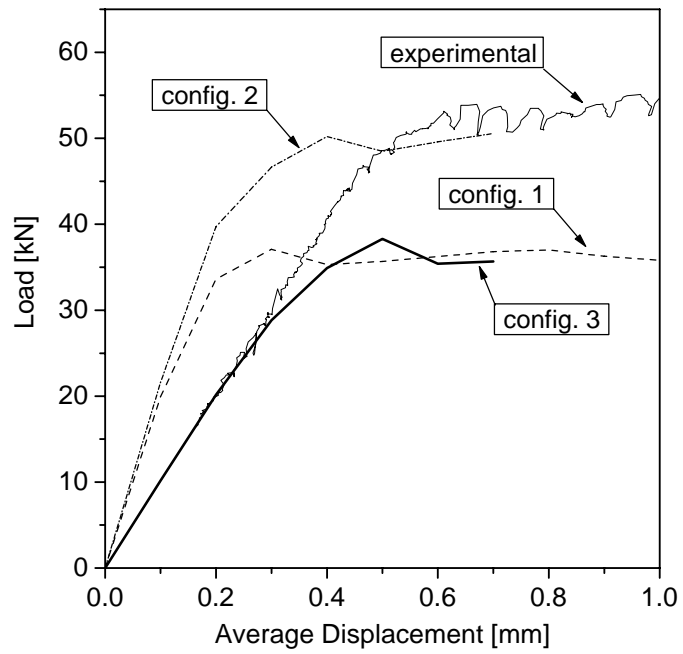
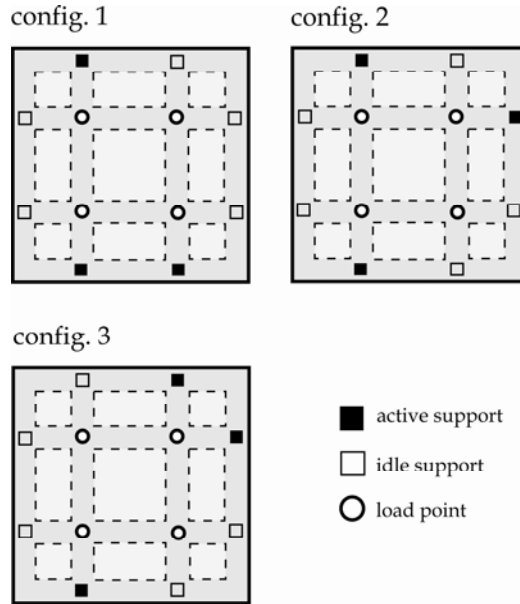


Fig. 6 -- Relationship between the total force and the average deflection at the loaded points.

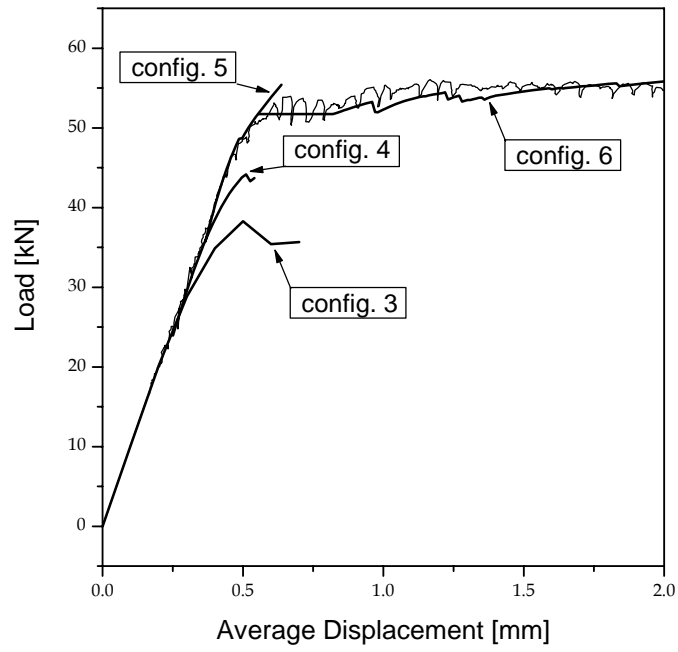
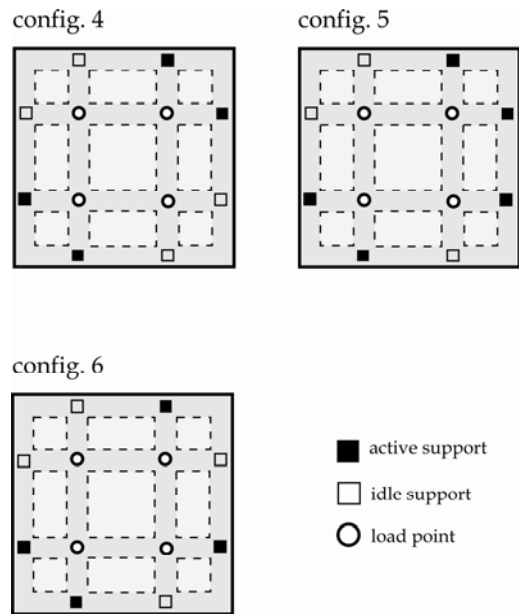


Fig. 7 -- Relationship between the total force and the average deflection at the loaded points.





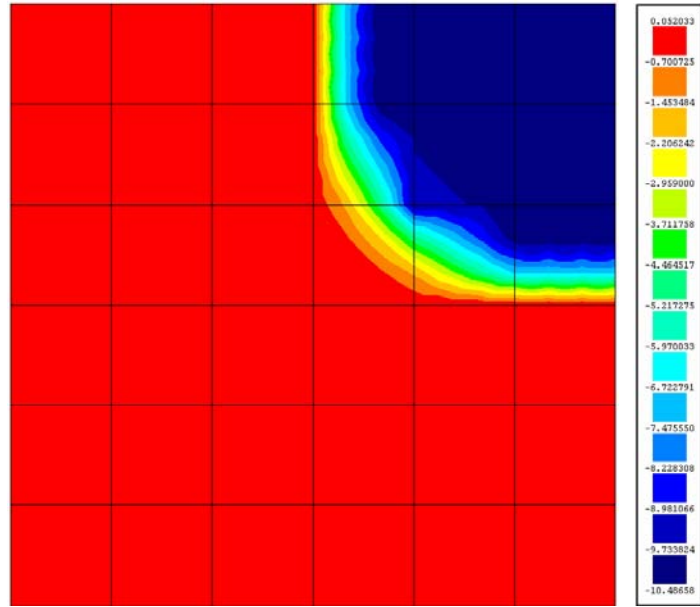


Fig. 12 -- Vertical displacement field (in mm) for the numerical simulation with out-of-plane shear softening (for a deflection of 10 mm in the center of the panel).



Fig. 13 -- Punching critical contour: a) top, b) and bottom faces.